Journal of Electrical Engineering and Information Technologies, Vol. **2,** No. 2, pp. 79–87 (2017)
Article 139
Received: August 22, 2017
Accepted: October 25, 2017
In print: ISSN 2545–4250
On line: ISSN 2545–4269
UDC: 004.421.6:621.316.937.052.6

Original scientific paper

HIGH FREQUENCY ENHANCEMENT OF THE HYBRID ELECTROMAGNETIC MODEL BY IMPLEMENTING COMPLEX IMAGES

Andrijana Kuhar, Vesna Arnautovski-Toševa, Leonid Grčev

Faculty of Electrical Engineering and Information Technologies,
"Ss. Cyril and Methodius" University in Skopje,
Rugjer Bošković bb, P.O. box 574, 1001 Skopje, Republic of Macedonia
kuhar@feit.ukim.edu.mk

A b s t r a c t: The well know hybrid electromagnetic model (HEM) is widely used for analysis of grounding systems. However, it has been proven that results obtained by HEM diverge from referent results in the high frequency (HF) domain. This paper presents implementation of complex image theory to take into account the earth-air interface instead of the quasi-static images used up-to-date with HEM. Parametric analysis of the achieved improvement in precision of the HEM method on high frequencies is visualized in multiple figures by comparison to referent results calculated by the renowned numerical electromagnetic code NEC-4. It may be concluded from the research presented in this paper that usage of complex images with HEM extends notably the applicability domain of the method.

Key words: hybrid electromagnetic model; complex images

ВИСОКОФРЕКВЕНЦИСКО ПОДОБРУВАЊЕ НА ХИБРИДНИОТ ЕЛЕКТРОМАГНЕТЕН МОДЕЛ СО ИМПЛЕМЕНТАЦИЈА НА КОМПЛЕКСНИ ЛИКОВИ

А п с т р а к т: Добро познатиот хибриден електромагнетен модел (HEM) често се користи при анализата на заземјувачки системи. Меѓутоа, докажано е дека резултатите добиени со употреба на HEM отстапуваат од референтните резултати во доменот на високи фреквенции (HF). Во овој труд, за да се земе предвид разделната површина меѓу земјата и воздухот, применета е теоријата на комплексни ликови наместо квази-стационарните ликови кои досега се користени во согласност со методот HEM. Параметриската анализа на подобрувањето на прецизноста на резултатите добиени со ХЕМ на високи фреквенции е претставена на повеќе графици во споредба со референтни резултати добиени со реномираниот нумерички електромагнетен код NEC-4. Презентираните резултати од истражувањето во рамките на овој труд водат до заклучок дека фреквенцискиот домен на применливоста на методот HEM е значително проширен со примена на комплексни ликови.

Клучни зборови: хибриден електромагнетен модел; комплексни ликови

1. INTRODUCTION

The hybrid electromagnetic model (HEM) is a circuit based method that incorporates propagation of electromagnetic fields in the extraction of equivalent circuit elements, developed by Visacro in 2002 [1]. The principle of circuit based methods is to represent the geometry and electromagnetic characteristics of any type of problem by electric circuit parameters. The obtained equivalent electric circuit is analyzed by circuit theory procedures. The HEM method has been implemented for analysis of grounding systems in [1]–[8]. The authors who have implemented the HEM method in [1]–[5] used the classical image method [9] to take into account the presence of earth/air interface. The

authors in [6]–[8] implemented HEM using the quasi-static approximation of the complete expressions for the Green's functions due to horizontal and vertical electric dipole (HED and VED, accordingly) placed in a finitely conducting half-space which will be elaborated in the following section. While HEM yields correct results for frequencies up to a couple of MHz, beyond this threshold there are discrepancies in the results compared to referent values [8]. The imprecision presented in [8] is in part due to the quasi-static approximation of the Green's functions which was the motivation to investigate the effect of using the complex image method as a more sophisticated approximation.

The complex image method was introduced for calculation of electromagnetic fields from a line current source placed above imperfect ground [10], [11]. The essence of the abovementioned method is to substitute the finitely conducting earth with perfectly conducting earth positioned on a new level denoted as *complex depth*, $d/2$ [12]. As a result it is possible to analyze the electromagnetic field by superposition of fields originating from the line current source and the image of the current source when it is placed above a perfectly conducting ground on level $d/2$.

The aim of this paper is to show the improvement in precision of the HEM method on high frequencies that can be achieved by implementation of complex image theory as opposed to the quasi-static images used up-to-date with HEM.

The paper will be organized as follows: section 1 – introduction of the HEM method and complex image theory; section 2 – theoretical basis of HEM and the quasi-static approximation of Green's functions; section 3 – application of complex image theory on grounding conductors; section 4 – parametrically organized results obtained by implementation of complex image theory with HEM in comparison to the quasi-static images used up-to-date, and discussion. The improvement of precision of HEM will be presented by comparison to referent full-wave results obtained by the well-known electromagnetic code based on the method of moments solution of the electric field integral equation for thin wires, NEC-4 [13].

2. HYBRID ELECTROMAGNETIC MODEL

In this paper HEM is implemented on a system consisted of a horizontal perfect conductor placed in imperfect ground.

In Figure 1 σ, $\varepsilon = \varepsilon_r\varepsilon_0$ and μ_0 are the conductivity, permittivity and permeability of the soil, while the according characteristics of the air are σ_0, ε_0 and μ_0. The length of the conductor is Λ and its radius is denoted by a. The electrode is divided in N fictitious segments whose length Δl has to be much larger that its radius a ($\Delta l > 10a$ is usually adequate) in order to maintain the conditions for the thin wire approximation. The middle segment of the conductor is the location of the excitation voltage source, V_s. The excitation voltage source amplitude equals 1 V and a couple of frequencies are investigated.

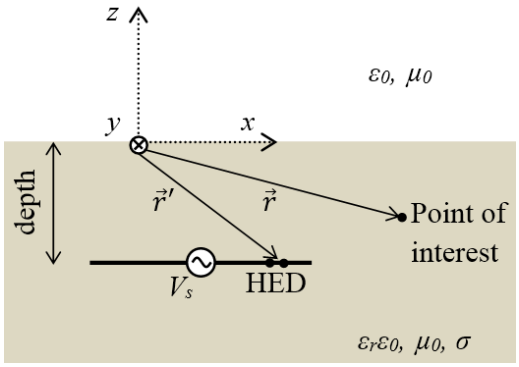

Fig. 1. Geometry of the conductor

Electromagnetic coupling between segments is evaluated from a numerical implementation of Maxwell's equations, obtaining longitudinal inductive circuit elements and transversal complex admittances [1]–[8]. The general expression for the equivalent inductivity of an arbitrarily positioned segment m, as obtained by HEM:

$$L_{mn} = \int_{\Delta l_m} \vec{t}_m \cdot \vec{t}_n \psi_A \left(\begin{matrix} l_-, l_+; m \\ n \quad n \end{matrix} \right) dl. \tag{1}$$

Transversal impedance between segments m and n as obtained by HEM.

$$Z^L_{m,n} = \frac{1}{4\pi(\sigma + j\omega\varepsilon)} \cdot \frac{1}{\Delta l_m \Delta l_n} \int_{\Delta l_m} \vec{t}_m \cdot \vec{t}_n \psi_V \left(\begin{matrix} l_-, l_+; m \\ n \quad n \end{matrix} \right) dl. \tag{2}$$

Equation (1) presents the influence of the longitudinal current through the source segment n, on segment m, while the influence of the leakage current exiting the source segment n on segment m (leakage impedances) is presented in (2). In (1) and (2):

$$\psi_{A,V}\left(l_{n_1}, l_{n_2}; m\right) = \int_{l_{n1}}^{l_{n_2}} G_{A,V}(n,m)dl' \,, \tag{3}$$

where G_A and G_V are the magnetic vector potential and electric scalar potential Green's functions for a conducting half-space, accordingly. Every source segment of the horizontal grounding conductor is treated as a horizontal electric dipole (HED). The complete expression for G_A due to HED is consisted of the following components:

$$G_A = \vec{i}_x\vec{t}_n G_{Ax} + \imath_x\vec{t}_n \cdot \imath_z\vec{t}_m G_{Az} \,, \tag{4}$$

where $\vec{t}_n$ and $\vec{t}_m$ are unit vectors defining the orientation of the source and target segment, accordingly.

Quasi-static approximation of Green's functions in a conducting half-space

The authors in [6]–[8] implemented HEM using the following quasi-static approximation of the Green's functions components in (4)

$$\begin{aligned} G_{Ax}^{x} &= \frac{\mu}{4\pi}\frac{\exp(-\gamma\rho)}{\rho}; \\ G_{Az}^{x} &= \frac{-\mu R_{1,0}\cos\varphi}{4\pi}\cdot\left\{\begin{array}{l}\exp[-\gamma(h-z)]- \\ -\cot\theta\dfrac{\exp\left(-\gamma\left|\vec{r}-\vec{r}\,^{i}\right|\right)}{\left|\vec{r}-\vec{r}\,^{i}\right|}\end{array}\right., \end{aligned} \tag{5}$$

where the distance between the source segment (HED) and segment of interest is $\rho = \left|\vec{r} - \vec{r}\,^{i}\right|$, r^i is the distance from the mirror image of the HED to the point of interest and $R_{1,0}$ is the quasi-static Fresnel reflection coefficient,

$$R_{1,0} = \frac{\underline{\varepsilon}_1 - \varepsilon_0}{\underline{\varepsilon}_1 + \varepsilon_0} \,. \tag{6}$$

Details of the remaining quantities in (5) can be found in literature [14]. The Green's function for the electric scalar potential originating from HED has the quasi-static form [14]:

$$G_V = \frac{1}{4\pi\underline{\sigma}}\left[\begin{array}{l}\dfrac{\exp(-\gamma\rho)}{\rho}+ \\ +R_{1,0}\dfrac{\exp\left(-\gamma\left|\vec{r}-\vec{r}\,^{i}\right|\right)}{\left|\vec{r}-\vec{r}\,^{i}\right|}\end{array}\right]. \tag{7}$$

The authors' approach in [6]–[8] is to substitute (5) and (7) in (1) and (2) accordingly and solve the integrals by extracting the term containing propagation as follows:

$$\begin{aligned} &\int_{\Delta l_m}\psi_A\left(l_n^-, l_n^+; m\right)dl = \\ &= \exp\left(-\gamma r_{mn}\right)\cdot\frac{\mu_0}{4\pi}\int_{\Delta l_m}\int_{\Delta l_n}\frac{1}{\rho}dl'dl, \\ &\int_{\Delta l_m}\psi_V\left(l_n^-, l_n^+; m\right)dl = \\ &= \exp\left(-\gamma r_{mn}\right)\cdot\frac{1}{4\pi\underline{\sigma}}\int_{\Delta l_m}\int_{\Delta l_n}\frac{1}{\rho}dl'dl. \end{aligned} \tag{8}$$

In (8) r_{mn} is the distance between middle points of the source and segment of interest. The approach in (8) ensures balance between accuracy and efficiency of the HEM algorithm.

In the next steps the HEM method employs two unique premises originally introduced by Otero [15], listed below:

1. The average electric potential of the segment is approximated as arithmetic mean value of the potentials of the nodes that define that segment. The first premise from [15] expressed in matrix form:

$$\begin{aligned} &[U] = [S]\cdot[V], \\ &\text{where } s_{i,j} = \left\{\begin{array}{l}1/2\,, \text{ if segment } i \text{ is} \\ \quad \text{conected to node } j; \\ 0, \text{ if segment } i \text{ is not} \\ \quad \text{connected to node } j\,.\end{array}\right. \end{aligned} \tag{9}$$

On the other hand, the average potential of the segment, U, is expressed via leakage impedances (2),

$$[U] = [Z^L]\cdot[I^L]. \tag{10}$$

2. The leakage current flowing from each segment into the soil is represented by two current sources attached to the nodes that define the segment. The matrix representation of the 2nd premise of [15]:

$$[I_S^L] = [S]^T\cdot[I^L]. \tag{11}$$

Conventional nodal analysis is performed combining (9)–(11) with Kirchoff's laws and yields the unknown values of the potential and current along every segment. Kirchoff's voltage law is expressed using segment inductances:

$$[V_S]+[A]\cdot[V]=j\omega[L]\cdot[I], \tag{12}$$

where $[A]$ is the conventional matrix of incidence and the elements of $[L]$ are of the form (1). Kirchoff's current law involves the leakage impedances from (2) and is expressed by

$$[I_S]=[I_S^L]+[A]^T\cdot[I]. \tag{13}$$

3. COMPLEX IMAGE THEORY

The complex image theory is based on substituting the finitely conducting earth with perfectly conducting earth positioned on a (complex) depth $d/2$ [12]. The electromagnetic field is then analyzed by superposition of fields originating from the line current source and the image of the current source when it is placed above a perfectly conducting ground on level $d/2$. The existence of the abovementioned complex depth and its mathematical meaning is thoroughly discussed in [16]. A general method for derivation of the complex depth for a current source placed in air above finitely conducting earth is elaborated in [10]. The author in [10] equates the wave impedances for normal incidence of a wave at earth's surface for finitely conducting earth placed at $z = 0$ and perfectly conducting earth placed at $z = d/2$. As a result, the following expressions for the complex depth are obtained:

$$d = 2/\eta, \tag{14}$$

where the term η for ground with relative permittivity ε_r is defined by:

$$\eta \approx \sqrt{j\omega\mu_0\sigma}, \qquad \sigma >> \omega\varepsilon_0\varepsilon_r$$
and
$$\eta \approx \frac{60\pi\sigma}{\sqrt{\varepsilon_r}} + j\omega\sqrt{\mu_0\varepsilon_0\varepsilon_r}, \quad \sigma << \omega\varepsilon_0\varepsilon_r \tag{15}$$

The complex image theory has been implemented on horizontal electrodes placed in imperfect soil in [17]–[19]. The authors in [18] and [19] implement a modification of the magnetic vector potential and electric scalar potential Green's functions for a conducting half-space, according to the principles from [10]–[12]. Complex image theory modification performed on the first component in Equation (4) results with [18]:

$$G_{Ax}^x \approx \frac{\mu_0}{4\pi}\left[\begin{array}{l} G_{11}-\dfrac{k_1^2-k_0^2}{k_1^2+k_0^2}G_{12}+ \\ +\dfrac{\exp\left(-jk_1\left|z+z'\right|A\right)}{\sqrt{\rho^2+(\left|z+z'\right|B)^2}}- \\ -\dfrac{\exp\left(-jk_1\left|z+z'\right|A\right)}{\sqrt{\rho^2+(d+\left|z+z'\right|B)^2}} \end{array}\right], \tag{16}$$

where G_{11} and G_{12} are associated to spherical waves with wave number k_1, due to HED and its image,

$$G_{11}=\frac{\exp\left(-jk_1\sqrt{\rho^2+\left|z-z'\right|^2}\right)}{\sqrt{\rho^2+\left|z-z'\right|^2}},$$
$$G_{12}=\frac{\exp\left(-jk_1\sqrt{\rho^2+\left|z+z'\right|^2}\right)}{\sqrt{\rho^2+\left|z+z'\right|^2}}. \tag{17}$$

The complex image form of the second component in (4) is expressed by [18]:

$$G_{Az}^x \approx -\cos\varphi\frac{\mu_0}{4\pi}\exp\left(-jk_1\left|z+z'\right|A\right)\cdot \left[\begin{array}{l} \dfrac{\sqrt{\rho^2+(d+\left|z+z'\right|B)^2}-(d+\left|z+z'\right|B)}{\rho\sqrt{\rho^2+(d+\left|z+z'\right|B)^2}}- \\ -\dfrac{\sqrt{\rho^2+(\left|z+z'\right|B)^2}-\left|z+z'\right|B}{\rho\sqrt{\rho^2+(\left|z+z'\right|B)^2}} \end{array}\right], \tag{18}$$

where the wave numbers equal

$$k_0^2=\omega^2\mu_0\varepsilon_0, k_1^2=k_0^2(\varepsilon_r-j\sigma/(\omega\varepsilon_0)).$$

The value of the complex depth in the case of a linear current source placed in imperfect ground has the form [19]:

$$d = 2/\sqrt{j\omega\mu_0(\sigma+j\omega\varepsilon_0\varepsilon_r)}. \tag{19}$$

In Equations (16) and (18) the constants A and B are found in [12] and equal 0.4 and 0.96, accordingly.

The Green's function for the electric scalar potential originating from HED has the complex image form [18]:

$$G_V = \frac{1}{4\pi\underline{\varepsilon}}\left[\begin{array}{l} G_{11} - \dfrac{k_1^2 - k_0^2}{k_1^2 + k_0^2} G_{12} + \\ + \dfrac{2\exp\left(-jk_1\left|z+z'\right|A\right)}{\sqrt{\rho^2 + (d+\left|z+z'\right|B)^2}} \end{array}\right]. \qquad (20)$$

4. RESULTS

The HF results obtained by implementation of complex image theory integrated with HEM in comparison to the quasi-static images used up-to-date will be parametrically presented in the following figures. In order to observe the HF improvement in precision of HEM the results are compared to referent values obtained by implementation of the renowned numerical electromagnetic MoM-based code NEC-4 [13].

Figure 2 presents comparison of current magnitude along a horizontal grounding conductor of 2 m length for various values of depth of burial and soil resistivity $\rho = 1/\sigma$. The excitation frequency is 5 MHz. Figure 3 presents comparison of results for the 2 m long horizontal grounding conductor at excitation frequency of 10 MHz. It is notable from Figure 2 that although slightly, the improvement introduced by complex image theory is more enunciated at 10 MHz. The current magnitude along a 5 m long horizontal conductor for various values of soil conductivity and depth of burial is visualized in Figures 4 and 5 for frequencies of 5 and 10 MHz, accordingly. Figure 6 presents comparison of current magnitude for a 10 m long horizontal grounding conductor for various values of the abovementioned parameters for excitation frequency of 5 MHz. Figure 7 presents comparison of results for the 10 m long horizontal grounding conductor at 10 MHz. Quasi-static results calculated by implementing (5)–(7) are denoted by 'Q-s.', results obtained by implementation of complex image expressions (16)–(20) are denoted by 'Cplx.' and the referent results by 'NEC4' in Figures 2–7. It is remarkable that in all of the studied cases except the 10 m long conductor (Figures 2–5), the results obtained by the complex image method converge perfectly towards referent results at 5 MHz. At the frequency of 10 Mhz the same can be concluded for 2 m and 5 m lengths in all cases except in the case of extremely resistive soil (ρ =1000 Ωm). In the latter case, the results are significantly improved, yet not a perfect match with the referent ones, which can be potentially explained by the vicinity of a resonant frequency.

In the case of a 10 m long conductor shown in Figures 6 and 7, it is evident that for ρ = 1000 Ωm there is an odd result less precise than the quasi-static image theory. The abovementioned irregularity might also be a consequence of a nearby resonant frequency for the length of question at 10 MHz, which is a matter to discuss in future papers.

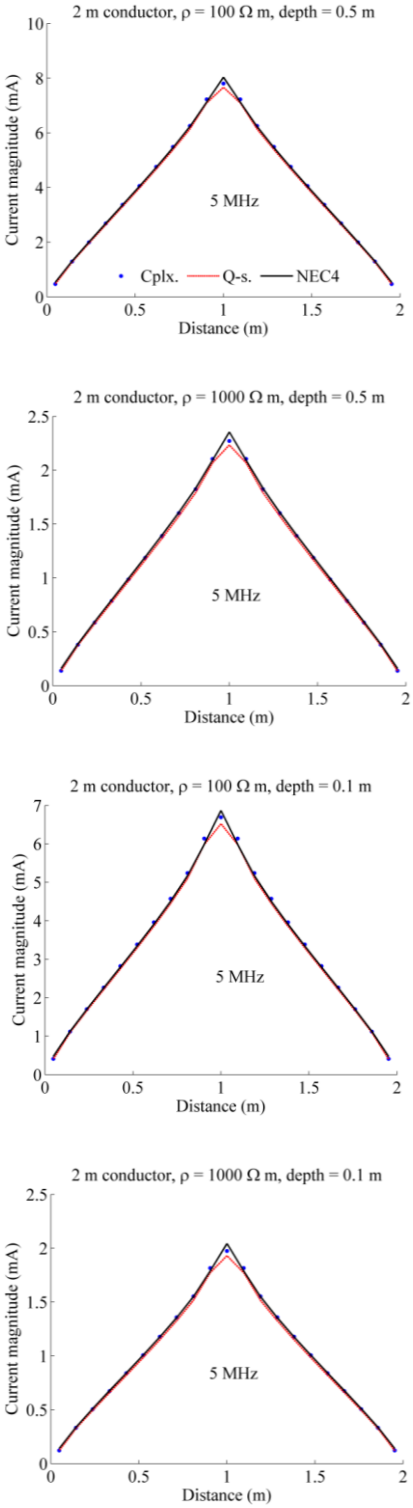

Fig. 2. 2 m long conductor at 5 MHz

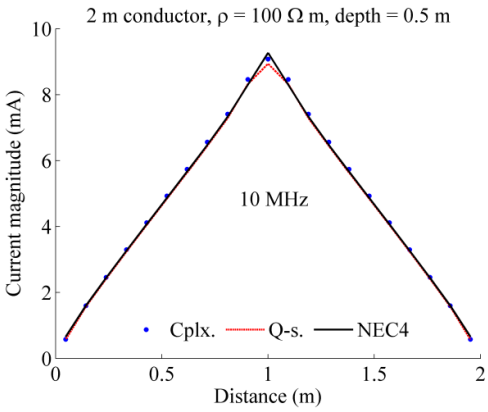

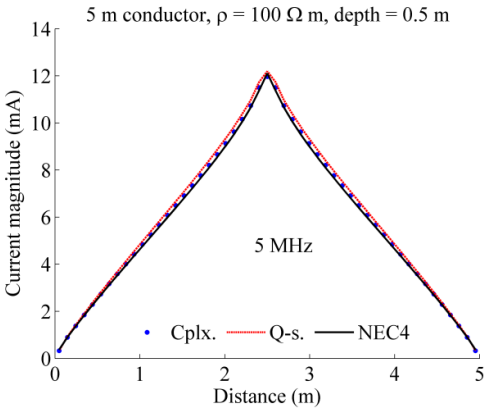

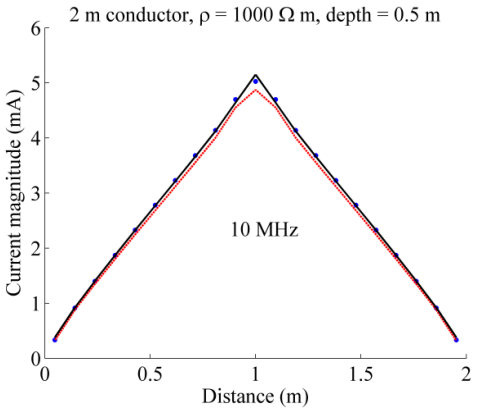

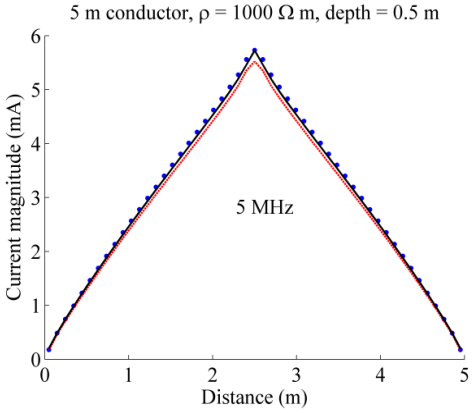

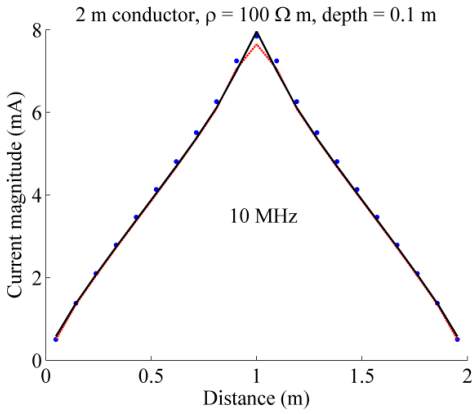

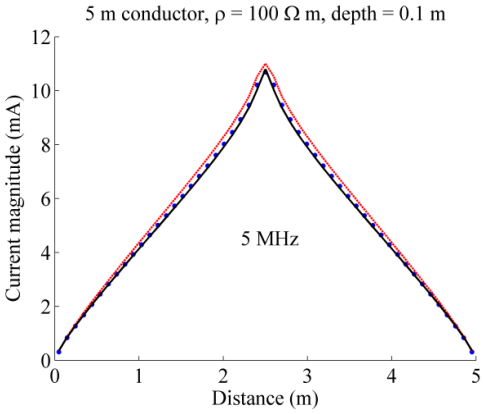

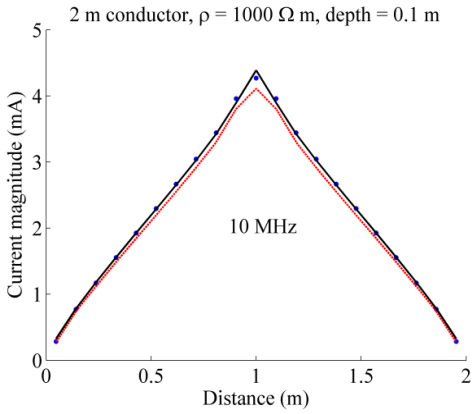

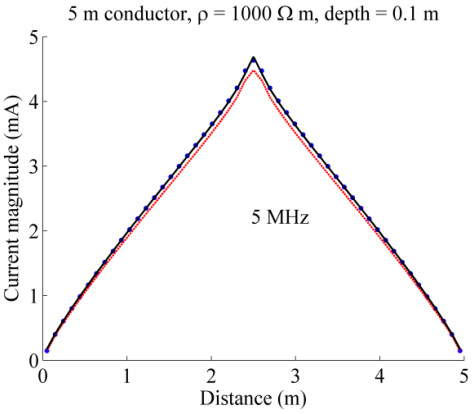

Fig. 3. 2 m long conductor at 10 MHz

Fig. 4. 5 m long conductor at 5 MHz

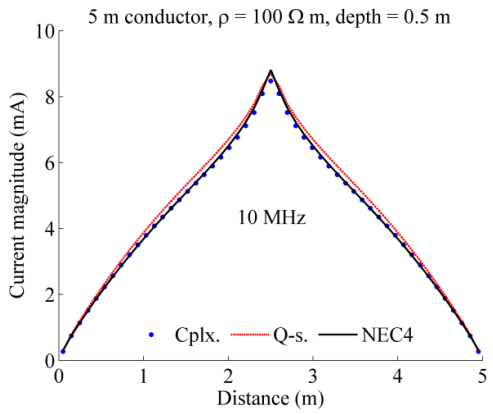

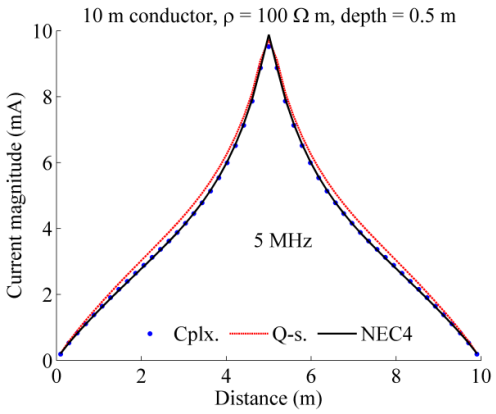

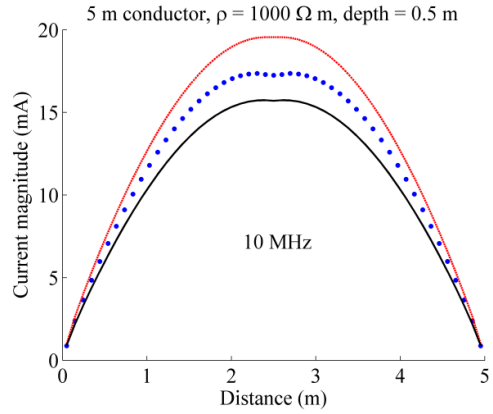

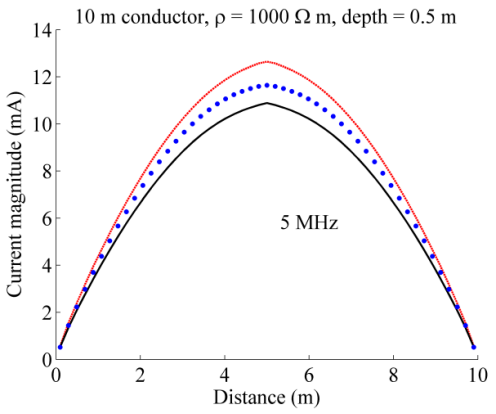

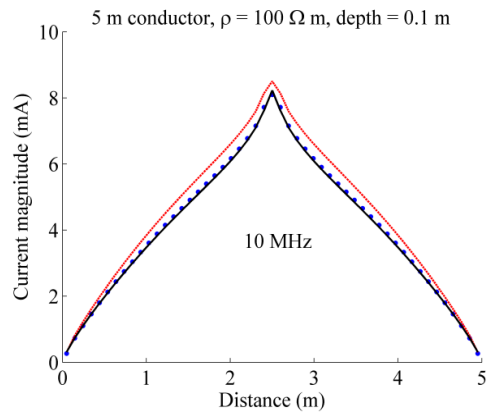

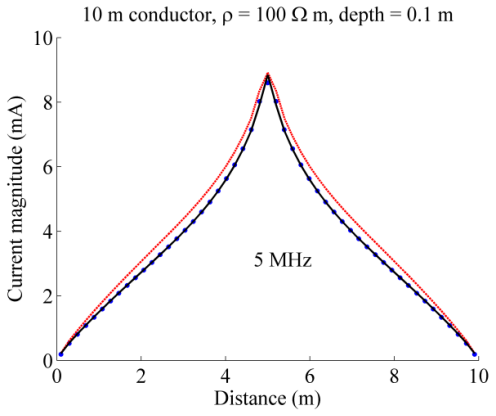

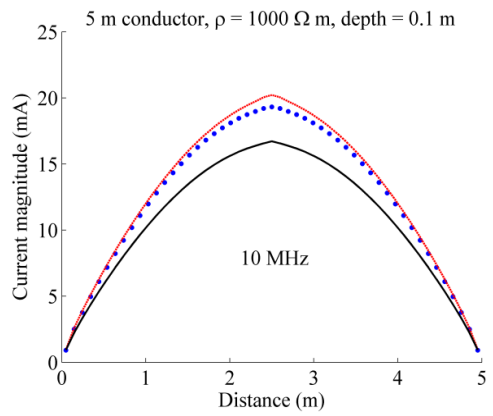

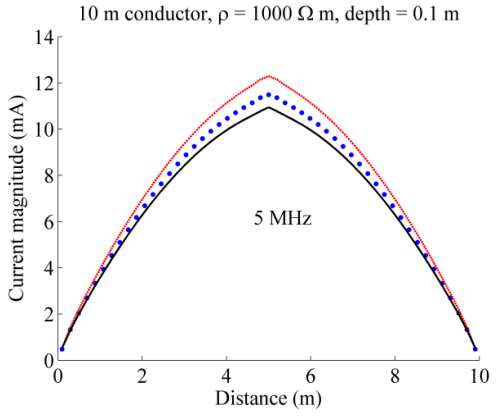

Fig. 5. 5 m long conductor at 10 MHz

Fig. 6. 10 m long conductor at 5 MHz

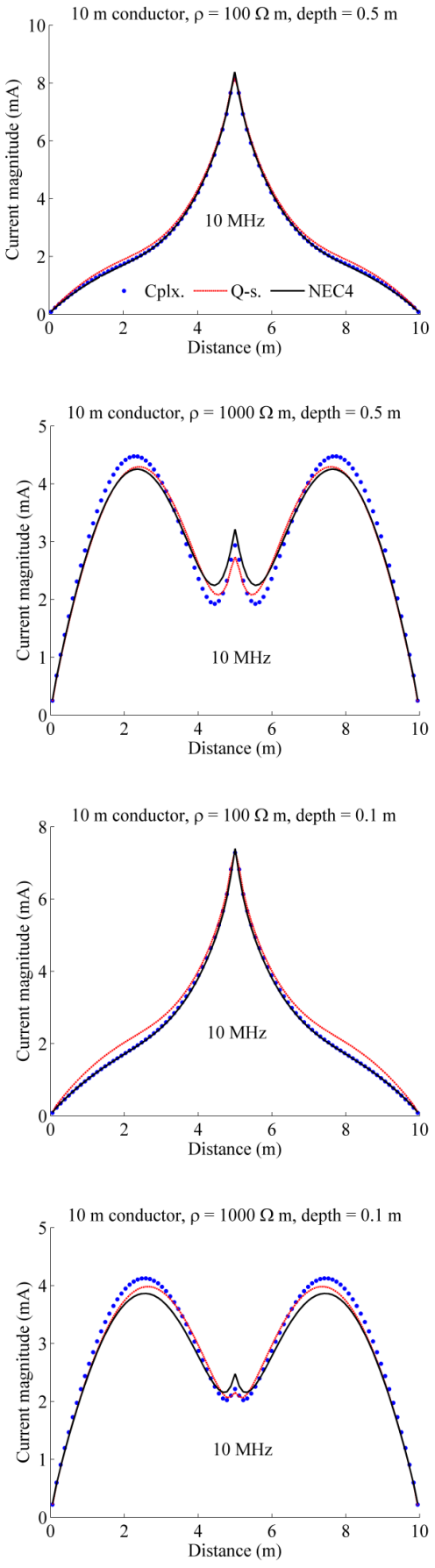

Fig. 7. 10 m long conductor at 10 MHz

REFERENCES

[1] Visacro S., Soares A. and Schroeder M. A.: An interactive computational code for simulation of transient behavior of electric system components for lightning currents, *Proc. 2002 Int. Conf. Lightning Protection*, pp. 732–737, 2002.

[2] Visacro S. and Soares A.: HEM: A model for simulation of lightning – Related engineering problems, *IEEE Trans. Power Delivery*, vol. **20**, no. 2, pp. 1206–1208, (2005).

[3] Guimarães M., Araujo L., Castro R. V., Santos L. F. D., Murta Vale M. H. and Visacro S.: Impulse response of grounding grids: Experimental versus simulated results, *Proc. 2012 Int. Conf. Lightning Protection*, 2012.

[4] Alípio R. S., Schroeder M. A. O., Afonso M. M. and Oliveira T. A. S.: Electromagnetic fields of buried conductors, *Proc. Int. Conf. Grounding Earthing (GROUND 2008)*, pp. 399–402, 2008.

[5] Alípio R. S., Schroeder M. A. O., Afonso M. M. and Oliveira T. A. S.: Electric fields of grounding electrodes: frequency and time domain analysis, *Proc. X International Symposium on Lightning Protection 9th–13th November, Curitiba, Brazil*, 2009.

[6] Kuhar A., Ololoska-Gagoska L. and Grčev, L.: Numerical analysis of complex grounding systems using circuit based method, *Proc. 12th Int. Conf. ETAI, Ohrid, Macedonia*, Sep. 2015.

[7] Jankoski R., Kuhar A. and Grčev L.: Frequency domain analysis of large grounding systems using hybrid circuit model, *Proc. 8th Int. PhD Seminar on Computational and Electromagnetic Compatibility – CEMEC, Timisoara, Romania*, Sep. 2014.

[8] Kuhar A. and Grčev L.: Contribution to calculating the impedance of grounding electrodes using circuit equivalents, *FACTA UNIVERSITATIS, Series: Electronics and Energetics,* vol. **29**, no. 4, pp. 721–732 (2016).

[9] King R. W. P.: Antennas in material media near boundaries with application to communication and geophysical exploration, Part I: The baremetal dipole, *IEEE Trans. Antennas Propag.,* vol. **AP-34**, no. 4, pp. 483–489, (1986).

[10] Watt A. D., Personal communication, 1962.

[11] Wait J. R., and Spies K. P.: On the image representation of the quasi-static fields of a line current source above the ground, *Can. Journal of Physics*, **47** (23), pp. 2731–2733, (1969).

[12] Bannister P.: Applications of complex image theory, *Radio Science*, vol. **21**, no.4, pp. 605–616 (1986).

[13] Burke G. J.: *Numerical Electromagnetics Code — NEC-4, Method of Moments,* Part II*: Program Description—Theory*, UCRL-MA-109338, Lawrence.

[14] Livermore National Laboratory, Livermore, 1992.

[15] Arnautovski-Toševa V. and Grčev L.: On the image model of a buried horizontal wire, *IEEE Trans. Electromagn. Compat.*, vol. **58**, no. 1, pp. 278–286 (2016).

[16] Otero A. F., Cidras J., Alemo J. L.: Frequency-dependent grounding system calculation by means of a conventional nodal analysis technique, *IEEE Transactions on Power Delivery*, Vol. **14**, No. 3, pp. 873–878 (1999).

[17] Park D.: Magnetic field of a horizontal current above a conducting earth, *J Geophys. Res*. **78** (16) pp. 3040–3043 (1973).

[18] Chow Y. L., Yang, J. J. and Srivastava, K. D.: Complex images of a ground electrode in layered soils, *Journal of Applied Physics* (1992).

[19] Arnautovski-Toševa V.: Approximate closed-form solution of the electric field due to HED within finitely conductive earth. In: *Proc. 2011 International Conference on Electromagnetics in Advanced Applications, ICEAA'11, Torino, Italy,* pp. 670–673, 2011.

[20] Arnautovski-Toševa V, Grčev L. and Kacarska M.: Applicability of approximate Green's functions in MPIE model of a horizontal wire conductor in lossy soil, *5th International Symposium on Applied Electromagnetics – SAEM'2014, Skopje, Macedonia*, 2014.